buildings

MDPI

Article

Uplift Behaviour of External Fibre-Reinforced Polymer Wrapping on RC Piles in Dry and Submerged Sandy Soil

Mohamed Younus Meeran Mydeen [1,*], Murugan Madasamy [1] and Bright Singh Seeni [2]

[1] Department of Civil Engineering, Government College of Engineering, Tirunelveli 627005, India; murugan@gcetly.ac.in
[2] Department of Civil Engineering, Mepco Schlenk Engineering College, Sivakasi 627005, India; brightsingh@mepcoeng.ac.in
* Correspondence: mohamedyounus@gcetly.ac.in

Abstract: The sudden occurrence of an earthquake induces a liquefaction effect on foundation soil, which causes a substantial increase in the uplift pressure acting on piles and causes structural damage to superstructures. This forms the basis of the necessity of experimenting with the behaviour of piles subjected to uplift loads and predicting their load-carrying capacity or resistance. Fibre-reinforced polymer (FRP) wraps are widely used for strengthening and retrofitting piles subjected to damage. The current study is aimed at determining the uplift load-carrying capacity or resistance of piles wrapped with basalt fibre-reinforced polymer (BFRP) and glass fibre-reinforced polymer (GFRP) sheets by experiment. Preliminary tests were conducted to identify the influence of BFRP and GFRP wraps on the mechanical strength properties of concrete. The mechanical strength of the specimen with the double wrapping of basalt and glass fibres in the perpendicular direction outperformed all other specimens. Moreover, the piles were wrapped with laminates and experimented on for their uplift capacity in dry and submerged conditions. The results indicate a considerable improvement in the uplift resistance of the piles compared with the unconfined piles. The BFRP and GFRP wraps improved the uplift resistance of the piles by 35.56% and 15.56%, respectively, higher than the unconfined pile for dry conditions. The angle of the interfacial friction in dry and submerged states was observed to be the maximum for the perpendicular direction for both of the FRP wraps, and the failure modes were compared. The simulated model showed a significant correctness for determining the uplift resistance of FRP-wrapped piles in dry and submerged states. The degree of agreement in the dry condition for the experimental results and finite element method was more than 94% for all fibre wraps.

Keywords: pile foundation; uplift resistance; fibre-reinforced polymers; glass fibre; basalt fibre

Citation: Meeran Mydeen, M.Y.; Madasamy, M.; Seeni, B.S. Uplift Behaviour of External Fibre-Reinforced Polymer Wrapping on RC Piles in Dry and Submerged Sandy Soil. *Buildings* **2023**, *13*, 778. https://doi.org/10.3390/buildings13030778

Academic Editor: Giuseppina Uva

Received: 20 February 2023
Revised: 8 March 2023
Accepted: 10 March 2023
Published: 15 March 2023

1. Introduction

Pile foundations are categorised under deep foundation, which finds application in carrying the loads of massive structures, especially in weaker soil conditions where shallow foundations cannot be constructed. Pile foundations are intended to act as a compressive member that resists vertical loads by transferring them through a weaker upper soil stratum with a low bearing capacity to a deeper stratum with a considerable bearing capacity [1]. Pile foundations find application in different forms of structures with more critical deployments in supporting heavier transmission line tower foundations, wharfs [2], coastal trestle bridges, and offshore wind power poles [3]. Liu et al. [4] mentions the usage of pipe piles for possessing superior dynamic response in offshore locations. The conventional materials used for the construction of piles include reinforced concrete, timber, and steel, which depend on the application and exposure conditions. However, conventional piles are susceptible to damage by axial and lateral loads, in addition to the damage from environmental exposure, which increases the demand for frequent repairs

and retrofitting [5,6]. The performance of piles often depends on the soil stratum that surrounds it [7]. Since pile foundations are driven or bored to a deeper stratum, passing through the weaker stratum, they generally face different interfacial conditions with soils, such as sand and clay in dry, saturated, or submerged conditions. In addition, piles are also affected by frost heave uplift, which induces major damage to the structure [8].

Externally bonded fibre-reinforced polymer composites are used to address the above issues, as it contributes to strengthening concrete piles and improving resistance to environmental factors [9]. Fibre-reinforced polymer (FRP) composites are increasingly used in many structural and geotechnical applications due to the fact of their high specific strength, light weight, durability, and resistance to chemicals and corrosive environments [10–12]. FRP is formed by the combination of two components, namely, the fibre, which is a reinforcing component, and a matrix component, such as epoxy, thermoplastic, and polyester [13]. The strengthening of severely damaged reinforced concrete exterior beam-column joints was investigated by [14] with the use of fibre-reinforced polymers and a fibre-reinforced cementitious matrix. FRP confinement on piles provides tensile strength in addition to its resistance against corrosion [13]. Carbon fibre-reinforced polymer (CFRP) is used for the repair of damaged structural members subjected to seismic forces due to the fact of their superior structural capacities and higher mechanical properties [15]. Vijay et al. [16] made use of GFRP composites for the restoration and rehabilitation of corroded submerged steel piles and estimated the repair cost to be 10 to 15% of the cost incurred for the replacement of the structure. CFRP has higher mechanical properties, excellent corrosion resistance, fatigue resistance, and creep resistance, especially in chemical and corrosive environments and loading [17]. In contrast, the Si-O skeletons of BFRP and GFRP may react with the alkaline solution of concrete, resulting in long-term performance degradation [18]. Therefore, different FRPs may be used according to different needs, such as cost performance, service environment, and bearing capacity [19]. Sharma et al. [20] observed an increase in the load-carrying capacity of columns by 89% and 149% for single and double wraps of GFRP, respectively. In addition, Vijayan et al. [21] observed an increase (approximately 5%) in the compressive strength of columns with an increase in the thickness of GFRP wraps from 0 to 5 mm. Basalt fibre, which is produced by the thermochemical extraction of volcanic rocks, provides superior mechanical, thermal, and chemical properties [22]. Ramaswamy et al. [23] observed a significant increase in the axial compressive strength of piles with the use of basalt fibre wraps for retrofitting.

During the occurrence of major earthquakes, the soil liquefies and loses its shear resistance against the uplift force. In such cases, a pile foundation is required to resist the uplift forces resulting from these actions, which are greater than the weight of the structure itself. Uplift forces can be the result of lateral loads acting on the structure. In this case, the bearing capacity of the pile depends on the soil resistance, and this dependence is termed soil–pile interaction [24]. The interaction between the soil and the structure needs to be analysed to understand the performance of piles subjected to earthquake loads [25]. The uplift capacity of a single pile is composed of suction generated at the base of the piles and the skin friction between the pile and soil, which is characterised by surface roughness. The theoretical analyses in [26] and [27] and the numerical analyses in [28–30] explain the uplift resistance or ultimate uplift capacity of vertical piles. Though various piles of different materials were subjected to uplift resistance tests, the influence of FRP laminates on the uplift resistance of piles used as surface wrappings of the piles remains unexplored. The current study aimed at determining the uplift resistance of piles wrapped with GFRP and BFRP laminates, along with its effect on the lateral load resistance. The novelty of the current research lies in experimenting with the real-time uplift behaviour of the original prototype piles cast with practical dimensions and subjected to general site conditions, such as dry and submerged states.

The following are the major highlights of this research:

- Understanding the effect of BFRP and GFRP laminate wrappings on the mechanical characteristics of concrete specimens subjected to compressive, tensile, and flexural loads;
- Determination of the angle of the interfacial friction based on the type of fibre and to understand the most positive orientation to achieve maximum improvement in the uplift resistance of the piles;
- Evaluating the influence of BFRP and GFRP wrappings on the uplift resistance of piles on sand under dry and submerged conditions;
- Comparison of the performances of BFRP- and GFRP-wrapped piles, with the unconfined piles subjected to uplift loads.

2. Materials and Methods

2.1. Preliminary Study

A preliminary study was conducted to determine the mechanical properties of the concrete specimen wrapped with BFRP and GFRP. The mechanical properties, such as compressive strength, split tensile strength, and flexural strength, were determined by destructive testing on cubes, cylinders, and prisms, respectively. In order to understand the mechanical behaviour of the FRP-confined concrete, concrete specimens were cast and then tested with and without FRP wrapping. The 28-day cured specimens were wrapped with unidirectional basalt and glass fibre-reinforced polymers with single and double plies. A set of three specimens pertaining to each mix was tested, and the average values were selected for an analysis of each's strength.

2.1.1. Material Properties

Before designing the mix, locally sourced, adulterant-free raw materials were tested according to Indian Standard codes.

Cement: OPC 53 grade cement adhering to the physical properties and chemical composition as per [31] the requirements was used for concreting. The specific gravity of the cement was 3.13, with a fineness value of 227 m^2/kg and a standard consistency of 31.2%. The initial and final setting times of the cement were 49 and 510 min, respectively. Moreover, the soundness of the cement obtained through an autoclave test was 0.3%. Table 1 tabulates the properties of the cement used.

Table 1. Cement Properties.

Property	Experimented Values	IS Codal Requirements [31]
Specific gravity (No Unit)	3.13	-
Fineness (m^2/kg)	227	≥225
Standard Consistency (%)	31.2	-
Initial Setting Time (min)	49	≥30
Final Setting Time (min)	510	≤600
Soundness (%)	0.3	≥0.8
Type and Grade	OPC 53	-

Fine aggregate (FA): Locally available natural river sand conforming to Zone II gradation of [32] the specification with a specific gravity of 2.61 and a fineness modulus value of 2.6 was used. The shape of the aggregates was observed to be angular, with a density of 1578 kg/m^3. Figure 1 shows the gradation curve of the fine aggregate.

Coarse aggregate (CA): Natural aggregate obtained from crushed granite stone conforming to a 20 mm size (specific gravity: 2.65) was taken from the local quarry. The angular-shaped aggregates were subjected to a series of tests to ensure their fitness for concreting. The gradation of the coarse aggregate can be observed in Figure 1. The combined index of the coarse aggregate was found to be 11.23%, which is less than the maximum limit of 40%, as mentioned in [33]. The properties of the fine and coarse aggregates are listed in Table 2.

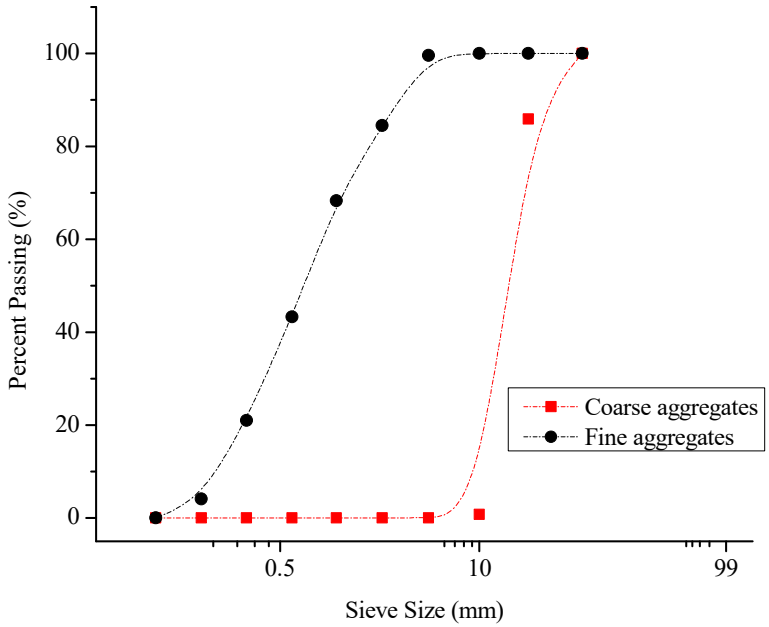

Figure 1. Gradation of the fine and coarse aggregates.

Table 2. Properties of the aggregates.

Property	Fine Aggregate	Coarse Aggregate
Gradation Zone	II	-
Source	River Sand	Local Quarry
Specific Gravity	2.61	2.65
Bulk Density (kg/m^3)	1578	1611
Combined Index (%)	-	11.23%

Concrete mix: Based on [34], M30 grade concrete was designed with a characteristic compressive strength of 30 MPa for casting of the specimens and pile elements. The constant mix proportion that arrived based on trials is tabulated in Table 3.

Table 3. Mix proportions.

	Grade	Cement	FA	CA	Water
Mix Proportion	M30	380 kg/m^3	730 kg/m^3	1041 kg/m^3	145 kg/m^3
Mix Ratio		1	1.92	2.74	0.42

FRP wrapping: Basalt fibre and glass fibre-reinforced polymer wraps were used in the study. The FRP sheets were prepared by a wet layup process [35], and their properties, obtained from the manufacturer, were provided in Table 4.

Table 4. Properties of the fibre laminates.

Properties	Thickness (mm)	Tensile Strength (MPa)	Elastic Modulus (GPa)	Ultimate Strain (%)	Fibre Thickness (mm)
BFRP	1	1450	51	1.6–3.0	1
GFRP	1.5	830	44	2.0–4.5	0.90

2.1.2. Casting of Specimens

The specimens intended for testing to determine the mechanical properties were prepared with the mix proportion mentioned in Table 3. A set of three samples representing

each mix was subjected to each test to ensure the accuracy of the results. In the case of tests on mixes with fibre wraps, a 28-day water-cured specimen (casted and cured at a standard temperature) was selected, and the surface was cleaned before the wrapping of the fibre laminates. During the wrapping, a coat of epoxy hardener in the prescribed dosage was applied uniformly on the surface of the specimen, followed by wrapping of the fibre laminates, and extra coats were applied between each ply of fibre and also on the surface to ensure the proper bonding of the wraps. The fibre-wrapped specimens were allowed to set under a standard temperature for three days and subjected to respective tests. However, one set of an unconfined concrete (conventional) specimen was also tested to compare the performance of the specimens with the fibre wraps. The identification of the mixes along with their specification are presented in Table 5.

Table 5. Details of the mixes.

Mix ID	Specifications
UC	Unconfined concrete
BF-PL-1	Unidirectional, single-ply BFRP-confined concrete with fibres parallel to loading
BF-PL-2	Unidirectional, double-ply BFRP-confined concrete with fibres parallel to loading
BF-PR-1	Unidirectional, single-ply BFRP-confined concrete with fibres perpendicular to loading
BF-PR-2	Unidirectional, double-ply BFRP-confined concrete with fibres perpendicular to loading
GF-PL-1	Unidirectional, single-ply GFRP-confined concrete with fibres parallel to loading
GF-PL-2	Unidirectional, double-ply GFRP-confined concrete with fibres parallel to loading
GF-PR-1	Unidirectional, single-ply GFRP-confined concrete with fibres perpendicular to loading
GF-PR-2	Unidirectional, double-ply GFRP-confined concrete with fibres perpendicular to loading

2.1.3. Compressive Strength Test

The test was performed in accordance with [36] on standard-sized cubes of the dimensions 150 × 150 × 150 mm. A compressive load of 140 kg/cm^2/minute was applied constantly until the occurrence of the ultimate failure of the specimen. A total of 15 cubes were tested among which three cubes pertained to the reference or unconfined mix. The compressive strength was determined based on the ratio of the compressive load applied to the corresponding cross-sectional area of the specimen.

2.1.4. Split Tensile Strength Test

The test was conducted in accordance with [37]. A standard test cylinder of a 300 mm length and a 150 mm diameter plain cement concrete was cast for this study. The experimental investigation was conducted on 15 cylinders, with three cylinders as the reference or unconfined mix. The tensile strength of the concrete cylinders was determined using the relation recommended in [37].

2.1.5. Flexural Strength Test

The test was performed based on the standard procedure mentioned in [36]. Plain cement concrete prisms of standard size (100 × 100 × 500 mm) were subjected to flexural loads at one-third span points. The supporting span of the prism was kept as 400 mm. The ultimate flexural load inducing the failure of the prisms was recorded, and the relationship mentioned in [36] was used for calculating the flexural strength.

2.2. Test on Piles

Following the results of the preliminary study, an M30 grade of concrete was incorporated along with steel reinforcements for the casting of pile elements followed by an exterior wrapping with fibre laminates. The particulars involved in the casting and testing of the pile elements are discussed below.

2.2.1. Test Tank

The test tank was designed to possess clear dimensions of 4.65 m × 2 m × 4 m for the placing of the pile elements, as shown in Figure 2. A series of 300 mm diameter (D) and 4 m long (embedded length was 3.1 m and free standing height was 0.9 m above ground level) bored cast in situ reinforced concrete piles were cast in the test tank. The piles were cast at a spacing of 1325 mm (4.4167 D). Figure 3 represents the schematic view of the pile setup.

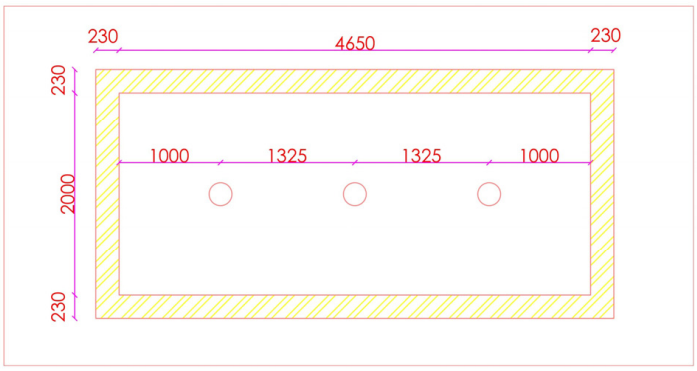

Figure 2. Model tank.

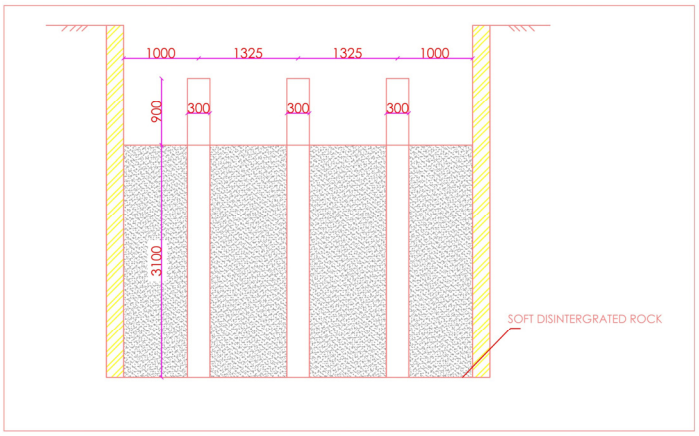

Figure 3. Schematic view of the pile setup.

2.2.2. Steel Reinforcement

For the casting of the piles, longitudinal and lateral steel reinforcements with a yield strength of 500 MPa were provided with an effective cover thickness of 40 mm. Six bars that were 12 mm in diameter were used as the longitudinal reinforcements of the piles, and bars that were 8 mm in diameter placed at 150 mm spacings were used as the lateral tie reinforcements.

2.2.3. Casting of Piles

The piles were cast within the test tank with the use of steel moulds for the placing of reinforcements and concrete. Steel reinforcement in the form of longitudinal main bars and lateral ties were designed as per [38]. Fabricated reinforcements were inserted in the bore holes, and the concreting was conducted with extensive care for providing uniform

compaction throughout the depth of the piles. The reinforcement was centred and sufficient cover (40 mm) was provided during the concreting. During the casting of the piles, the concrete was subjected to vibro-compaction every 300 mm in height in order to achieve the proper meshing of the concrete layers along with a good surface finish.

Curing: The piles were covered with gunny bags for water curing immediately after demoulding, since gunny bags can hold water for a long time. The wetness of the gunny bags was retained by damping them at regular intervals. The water curing was carried out for a period of 28 days under standard conditions for avoiding the loss of water.

2.2.4. FRP Wrapping

After the water curing, the elements were dried and surface cleaned using sand paper and a chisel. Furthermore, the elements were wrapped with FRP laminates around the surface with the aid of epoxy resins. The first coat of saturant was applied on the piles after providing a primer coat, and the FRP sheet was then confined directly on the surface. Extensive attention was paid to avoid the formation of voids between the FRP sheet and concrete surface. A special roller was used to remove the entrapped air bubbles and to press the resin to penetrate into the fabric. The roller was continuously used until the resin was reflected on the fabric surface, which indicates the complete wetting of the fibres. Finally, a resin layer was used on the surface of the confined piles. The FRP layer was confined around the pile with an overlap of one-fourth of the perimeter to avoid sliding or debonding of the fibres during tests. The confined piles were left at room temperature for 7 days to ensure the adequate hardening of the epoxy followed by the filling of sand. Figure 4 provides a flow chart for the sequence of works carried out to prepare the piles for subjecting to uplift load resistance tests, and Figure 5 shows the casting of the FRP-wrapped piles in this study.

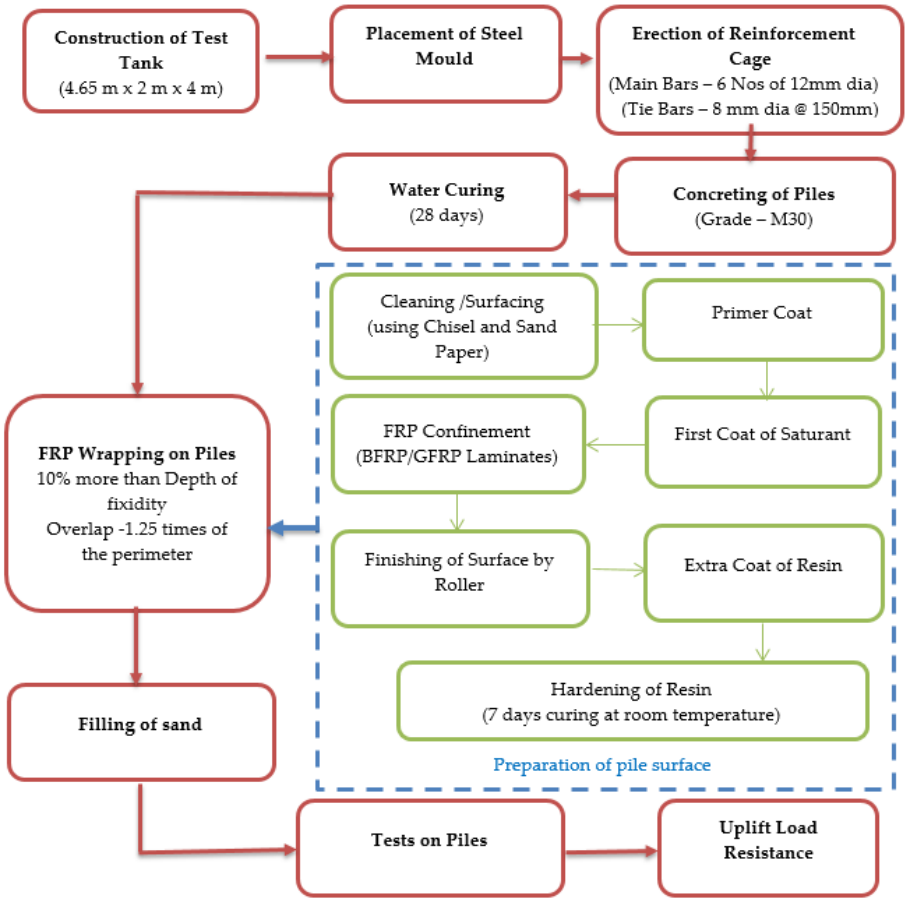

Figure 4. Casting and testing of the FRP-wrapped piles.

Figure 5. Casting of the FRP-wrapped piles: (**a**) placement of the reinforcement and concreting; (**b**) curing with wet gunny bags; (**c**) FRP wrapping; (**d**) coating of the epoxy above the FRP.

2.2.5. Soil Condition

Poorly graded sand with a fineness modulus of 2.50 was filled and placed surrounding the piles before conducting the experiment. Based on the applicable Indian Standard (IS) Codes, the properties of the soil were determined through a series of in situ and laboratory tests using disturbed and undisturbed samples, and they are listed in Table 6. The modulus of elasticity (E) was calculated for the sandy soil by the relation E = 300 (N + 6), where N is obtained from the standard penetration test (SPT) [39]. The soil was compacted in three layers, with the first layer from 0 to 1.0 m, the second layer from 1.0 to 2 m, and third layer from 2 to 3.1 m from the datum with the help of a rammer. Wet and dry sieve analyses were carried out for determining the particle size distribution curve. The particle size distribution curve is shown in Figure 6.

Table 6. Soil properties.

IS Classification	D_{10} (mm)	Cu	Cc	Natural Moisture Content (%)	Bulk Unit Weight (kN/m^3)	Maximum Dry Density (kN/m^3)	Minimum Dry Density (kN/m^3)	Specific Gravity
SP (Poorly Graded Sand)	0.24	3.42	0.85	17.14	16.28	16.64	15.37	2.64

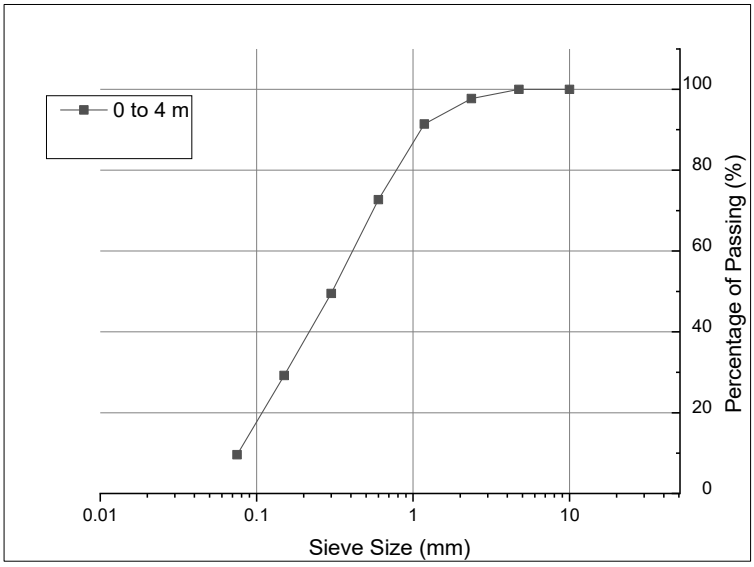

Figure 6. Particle size distribution of the soil.

2.2.6. Depth of Fixity

The depth of fixity of the pile was calculated in accordance with [40]. The depth of fixity is largely affected by the stiffness of the soil and pile material. Hence, the relative stiffness factor (T) was calculated according to the following relationship.

$$T = \left[\frac{EI}{k_1}\right]^{\frac{1}{5}} \quad (1)$$

where EI represents the flexural rigidity of the pile, and k_1 represents the coefficient of the subgrade reaction. Based on the values of the angle of the internal friction (Φ) and SPT value (N), the value of the coefficient of the subgrade reaction (k_1) was taken as 21 N/cm^2, as per Table 1 of IS 2911 (Part 1) [40]. In general, the failure of long flexible piles will occur at the level of depth of fixity due to the higher bending moment. Therefore, the depth of the FRP wrapping was planned to be 10% beyond the depth of fixity (1.5 m), which is approximately 1.65 m below the ground level.

2.2.7. Interface Behaviour between Soil and FRP Laminates

The uplift behaviour of the piles is largely dependent on the soil–structure interaction due to the frictional characteristics. The interfacial frictional characteristics of the investigated fibre laminates were determined by casting the concrete specimens (size 60 mm × 60 mm × 14 mm) and wrapping the fibre sheets and then subjecting them to shearing resistance tests using a standard direct shear apparatus. In the test mould, the prepared specimen was placed in the lower part of the shear box, and the test sand used for the uplift resistance test was placed on the upper part of the shear box before subjecting it to a direct shear test. A schematic representation of the test setup is displayed in Figure 7.

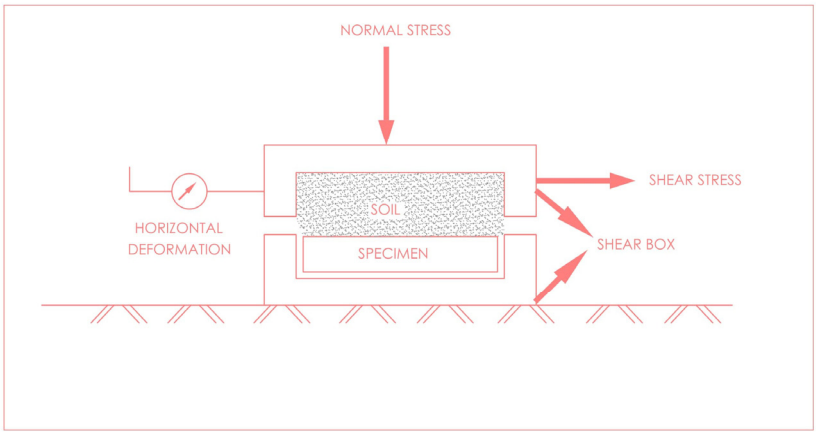

Figure 7. Experimental setup—interfacial friction angle.

2.2.8. Test for Uplift Load Resistance

The axial pull-out load was applied to the pile using a hydraulic jack that was supported by a steel section. Steel beams acted as a support between the reinforcement such that the beam acted as a platform for the hydraulic jack. The pull-out test was carried out on three RC piles as per [41]. The test setup for the reaction was assembled as shown in Figure 7. A hydraulic jack of a 50 T capacity was placed between the top of the pile reinforcement and the main girder. The packing plates were used to provide the necessary support between the loading jack and the pile. When the load was given to the hydraulic jack, it pushed up the reinforcement frame so that the pile was pulled out and the reaction was transferred through the steel beams. The reinforcement framework was capable of lifting the pile through the hydraulic jack. To measure the displacement of the pile, dial gauges of a 0.01 sensitivity were placed. The installation of the reaction girder and dial gauge and the experimental setup are shown in Figure 8.

The loads were applied to the nonextensible steel reinforcement, which was cast into the pile by means of a weld. Two dial gauges were fixed in the pile, equidistant from the axis of the piles. The loads corresponding to each unit of deflection were observed from both of the dial gauges. The average value of the displacement was recorded for both dial gauges, where the vertical displacement of the pile corresponded to the pull-out load applied by the hydraulic jack. The load and displacement values were noted at regular intervals.

2.2.9. Model Simulation

The behaviour of the pile was investigated using Plaxis, a finite element (FE) software package to compare the results from the experimental study. A concrete damage plasticity model was used to model the concrete piles. The structure–pile was modelled as a linear elastic nonporous material obeying Hooke's law having a compressive strength of 30 MPa, and the soil layer was assumed to be loosely saturated sand having an overlaying rigid rock. The Mohr–Coulomb model was implemented for the sand in the case of static analysis. The depth of the soil continuum was taken as 1.75 times [42] to eliminate the boundary effects. Infinite elements at a far distance were also observed to help eliminate the boundary effects [43]. A medium mesh with a lower coarseness factor of 0.25, which provided satisfactory results in recent studies [44–46], was selected (Figure 9). The interfaces were defined around the sides and underneath the pile with the material properties from adjacent soil and a strength reduction factor of $R_{inter} = 1$.

(**a**)

(**b**)

(**c**)

(**d**)

(**e**)

Figure 8. Uplift resistance test setup: (**a**) welding of the reinforcement; (**b**) installation of the reaction girder; (**c**) installation of the dial gauges; (**d**) final setup in a dry state; (**e**) final setup in a submerged state.

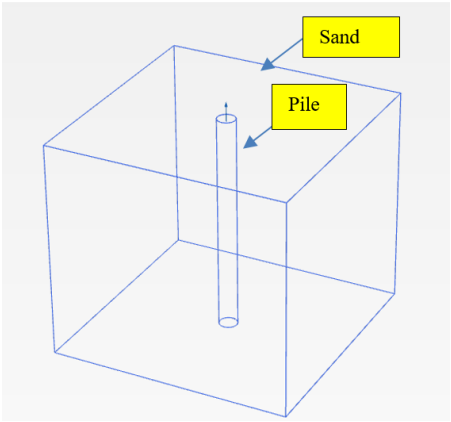

Figure 9. Mesh discretisation.

Around the pile model, a positive interface element was made to connect the pile around the sand bed in the finite element (FE) model. In addition, the side boundaries were constrained in the horizontal direction, and the bottom boundaries were constrained in both the horizontal and vertical directions. Figures 10 and 11 depict the numerically modelled pile considered for the validation, with the details of the mesh incorporated. The properties reported in Tables 3 and 4 were used to model the fibre-reinforced pile and the sand bed.

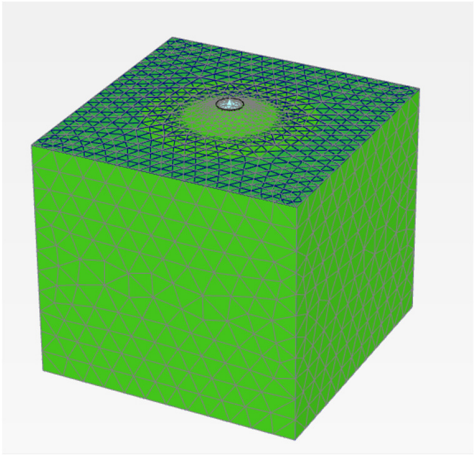

Figure 10. Deformed mesh.

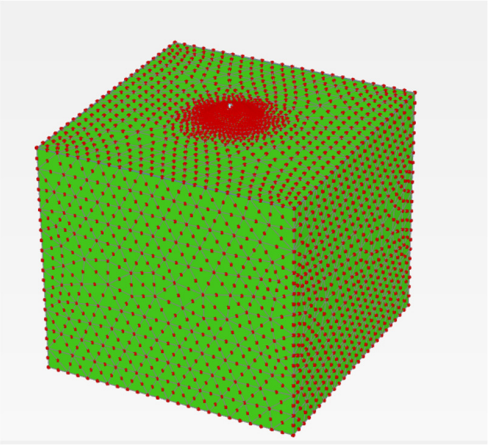

Figure 11. Generated mesh.

3. Results and Discussion

3.1. Mechanical Strength

The ultimate failure of the wrapped specimen was observed to occur due to the rupture of the fibre wrap. However, observation of the failed specimen showed that the failure of the confined concrete was initiated before the ultimate failure. The failure of the unconfined specimen was initiated with the crack formation at its soffit where compression prevails and multiple cracks occurred. For the confined specimen, the cracks initiated in proximity to the FRP wraps. In the case of the flexural specimen, the failure of the specimen occurred after showing ductile behaviour. The cracks of the confined specimen were smaller in width compared to the unconfined specimen due to the restraining effect of the wraps. This was found to be caused by the confining effect of the wrap along with their capacity to withstand higher loads, which hindered the change in the volume of the concrete specimen.

The compressive strength of the concrete cubes pertaining to the unconfined mix was observed as 38.25 MPa (Table 7) after 28 days of water curing under standard conditions. Furthermore, the wrapping of the BF on the surface caused a considerable increase in the compressive strength of the cubes. It can be observed from Figure 12 that the single wrapping of the cubes with BF in the parallel and perpendicular directions to the loading caused an increase in the compressive strength by 19.95% and 44.99%, respectively. However, the increase in the compressive strength was observed to be 40% and 90.01% for the double wrapping in the parallel and perpendicular directions, respectively, with respect to the loading direction.

Table 7. Mechanical properties.

Mix ID	Compressive Strength (MPa)	% Increase Compared with UC	Split Tensile Strength (Mpa)	% Increase Compared with UC	Flexural Strength (Mpa)	% Increase Compared with UC
UC	38.25	-	4.12	-	4.16	-
BF-PL-1	45.88	19.95%	5.56	34.95%	5.58	34.13%
BF-PL-2	53.55	40.00%	7.04	70.87%	7.10	70.67%
BF-PR-1	55.46	44.99%	6.78	64.56%	6.86	64.90%
BF-PR-2	72.68	90.01%	8.73	111.89%	8.81	111.78%
GF-PL-1	42.08	10.01%	4.94	19.90%	4.98	19.71%
GF-PL-2	45.84	19.84%	5.77	40.05%	5.79	39.18%
GF-PR-1	49.72	29.99%	5.97	44.90%	6.11	46.88%
GF-PR-2	61.20	60.00%	7.74	87.86%	7.78	87.02%

The split tensile strength of the unconfined mix was identified as 4.12 MPa, which is approximately 10.77% of its compressive strength. With the increase in the number of plies of BF, the split tensile strength was found to increase for both orientations. The higher tensile modulus of the BFRP wraps are the reason behind this increase in the tensile properties of the concrete. The split tensile strength of the cubes with single and double wraps of BF parallel to the loading direction were observed to be 34.95% (5.56 MPa) and 70.87% (7.04 MPa), respectively, higher than the unconfined mix. However, a major improvement was observed for the plies in the perpendicular direction, i.e., for the single and double plies, the increase in the split tensile strength was recorded as 64.56% (6.78 MPa) and 111.89% (8.73 MPa), respectively (Figure 13). Moreover, the ratio of the split tensile strength to the compressive strength was observed to be the lowest (12.01%) for the BF-PR-2 specimen due to the substantial increase in both the compressive strength and split tensile strength.

The flexural strength of the concrete was observed to be 4.16 MPa, which is approximately 10.88% of its compressive strength. The flexural strength was observed to increase in a pattern similar to that of the tensile strength. The maximum flexural strength was recorded as 8.81 MPa for the BF-PR-2 specimen, which is 111.78% higher than the unconfined specimen. The BFRP wrapping in parallel to the loading direction also caused an

increase in the flexural strength by 34.13% and 70.67% for the single and double wraps, which is 18.66% and 19.41% less than that of the perpendicular plies (Figure 14).

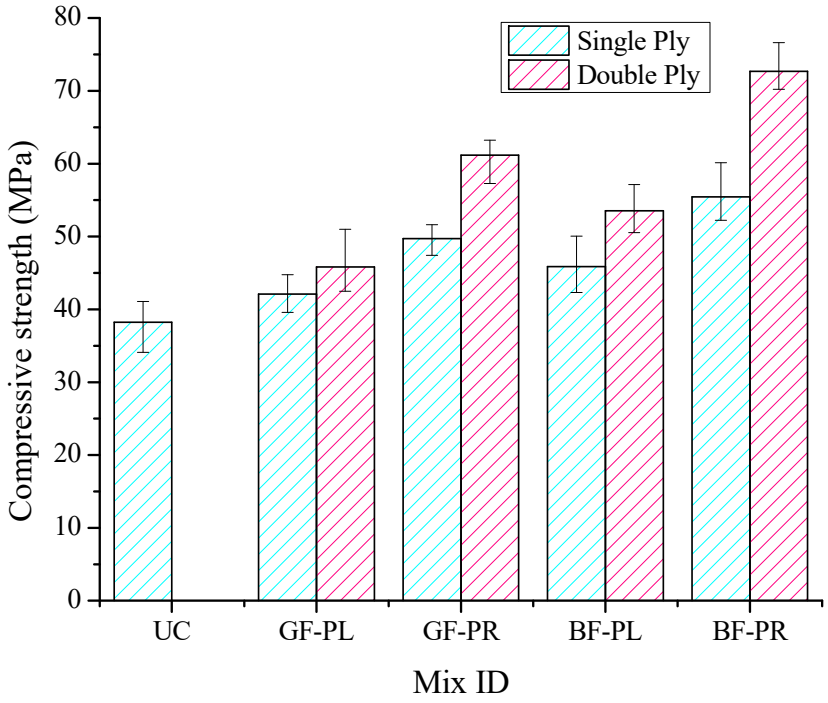

Figure 12. Compressive strength.

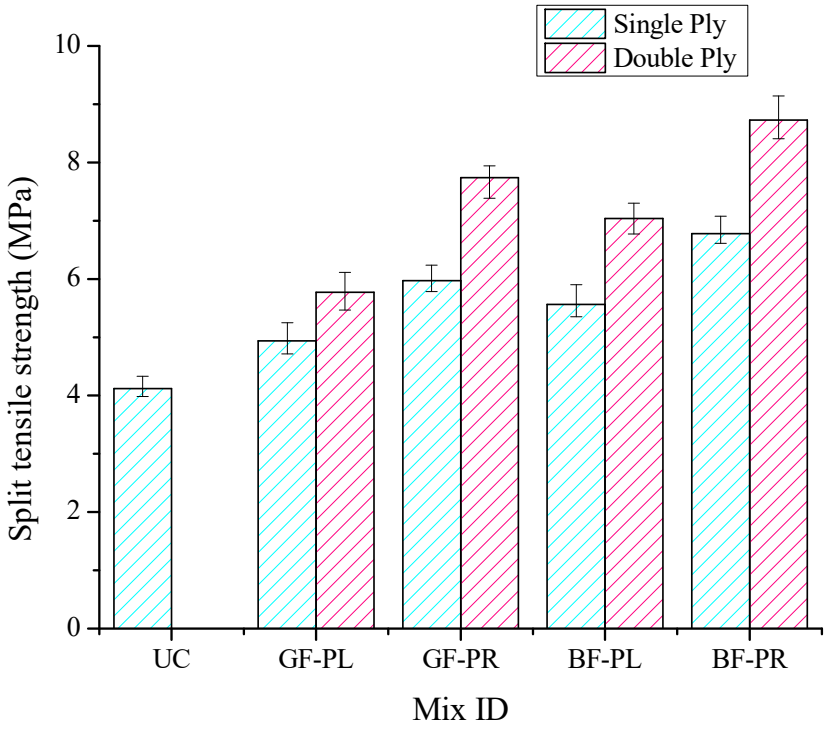

Figure 13. Split tensile strength.

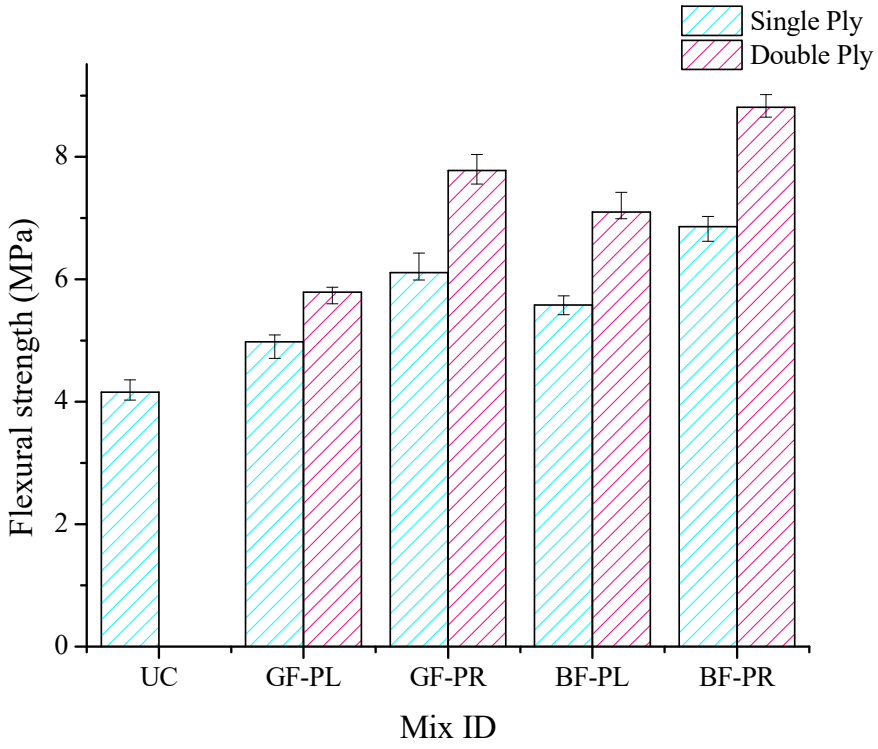

Figure 14. Flexural strength.

3.2. Interfacial Friction between Soil and Surface of Piles

The interfacial friction between the soil and the surface of the piles was examined using a direct shear testing apparatus, and the interfacial friction with respect to the direction of the fibre orientation of the laminates is presented in Table 8. From Table 8, it can be observed that all specimens with FRP wrapping showed a higher angle of interface friction compared to the normal concrete specimen (UC) due to the roughness induced by the fibre laminates. This shows that the potential for increasing the uplift resistance of the piles improves with the FRP wrapping. Moreover, the angle of the interfacial friction of the basalt fibre sheets was observed to be higher than that of the glass fibre sheets for both directions of the fibres. Among the investigated specimens, the specimen with a fibre orientation parallel to the loading direction showed a lower interfacial friction angle compared to the specimen with a fibre orientation perpendicular to the loading direction irrespective of the type of fibre wrap. The maximum of the interfacial friction angle among the investigated specimens was recorded as 38.26 ° for the BF-PR-1 specimen, which had a basalt fibre oriented in the direction perpendicular to the loading direction. However, it is noted that the double wrapping of fibres for both fibre types showed insignificant or no influence compared to the effect of the single wrapping. The interfacial frictional behaviour plays a predominant role in defining the uplift resistance of the piles rather than the mechanical strength of the piles or the number of fibre wraps.

3.3. Uplift Resistance

During the uplift load test, the surrounding soil was found to deform along the sides of the piles. Hence, the soil deformation patterns around the piles were observed carefully by spreading white chalk powder. A clear gap was observed to exist between the pile and the surrounding soil during the application of the uplift pressure. This clear gap was found to be extended beneath the surface of the soil along the surface of the piles. However, the thickness of the gap was found to decrease with the increase in the depth up to a critical depth beyond which no gap was observed. This may be due to the increase in the unit skin friction at the interface between the soil and pile surface up to the critical depth beyond which it remained constant [47]. Soil deformation patterns around the pull-out test piles

and pile–soil interactions were observed. It is quite obvious that there was a clear gap between the pile and the surrounding soil surface in the upward loading side of the ground. This clear gap was extended to some depth below ground level depending on the type of FRP wrapping. Considering Figures 15 and 16, the maximum displacement occurred in the ground surface and decreased gradually with depth. As per [41], the safe load shall be taken as two-thirds of the load at which the total displacement is 12 mm or half of the load at which the load–displacement curve shows a clear break.

Table 8. Angle of the interfacial friction.

Specimen	Interface Type	Angle of Interfacial Friction Dry State	Angle of Interfacial Friction Wet State
-	Sand–sand	35.31°	28.95
UC	Sand–concrete	33.87°	28.11
GF-PL-1	Sand–0° GFRP-wrapped specimen	36.11°	30.87
GF-PR-1	Sand–90° GFRP-wrapped specimen	37.78°	31.92
BF-PL-1	Sand–0° BFRP-wrapped specimen	37.54°	31.47
BF-PR-1	Sand–90° BFRP-wrapped specimen	38.26°	32.32

Figure 15. Gap between pile and soil.

Figure 16. Deflection of the piles during the uplift.

However, the safe load of the pile was taken as the least of these two values. The load versus displacement, commonly known as p-y, is represented in the graph (Figure 17). The GFRP and BFRP piles were found to be better performing than the unconfined piles during the uplift loading. The failure envelope of the piles when subjected to the uplift loads is provided in Figure 18 which primarily depends upon the surface roughness of the piles. The diameter of the wedge extended during the uplift was observed as 1.14 m for the unconfined piles, whereas for the GFRP- and BFRP-wrapped piles, it extended up to 1.40 m and 1.52 m, respectively. The wedge angle was observed to be 73°, 69°, and 67° for the unconfined, GFRP-, and BFRP-wrapped piles, respectively. The observed wedge for all piles were similar to the observation in [27].

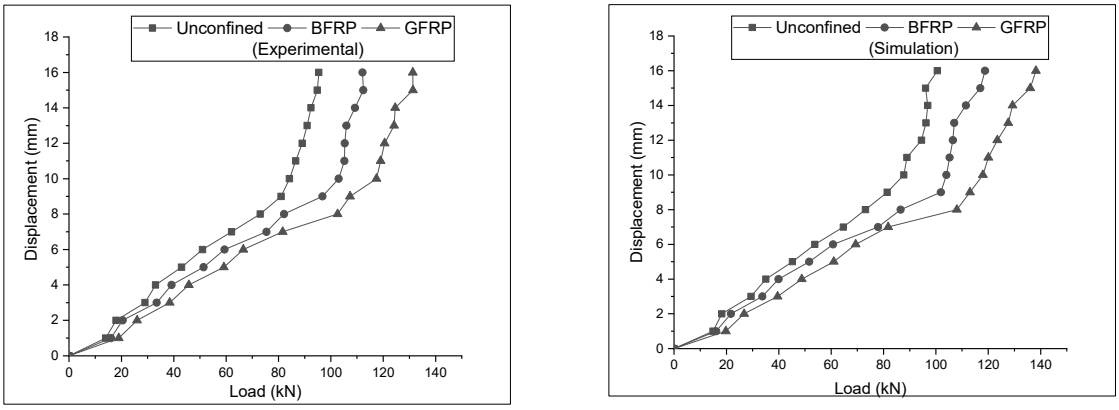

(**a**) (**b**)

Figure 17. Load vs. settlement (dry state): (**a**) Experimental (**b**) Simulation.

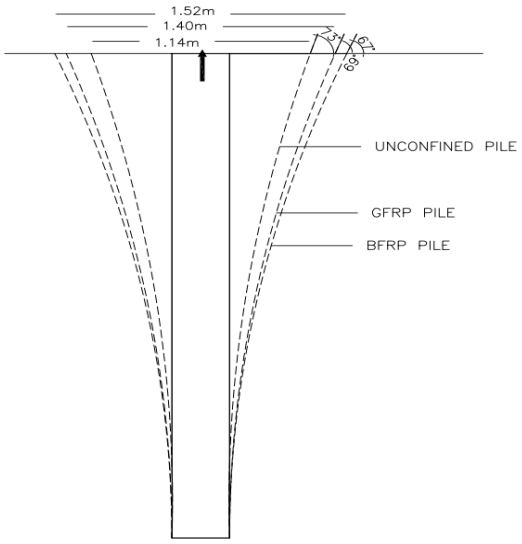

Figure 18. Failure envelope during the uplift.

3.4. Comparison of Experimental and Simulation Data

The load displacement diagram of the pile subjected to the uplift loading based on the finite element analysis is shown in Figure 19. From the experimental study, the ultimate uplift capacity of the unconfined pile was found to be 59.4 kN. The glass fibre-reinforced polymer (GFRP) and basalt fibre-reinforced polymer (BFRP) showed a higher strength than the unconfined pile (Figure 20). The ultimate uplift capacity was observed as 80.52 kN and 68.64 kN for the piles with the GFRP and BFRP wraps, respectively, which is 35.56% and 15.56% higher than the unconfined pile. The increase in the uplift load-carrying capacity

was influenced by the pile surface texture, which is dictated by the weaving of the fabric, imparting a higher skin frictional resistance on the interface. The GFRP imparted a higher surface roughness compared to the BFRP and, hence, resulted in a higher uplift capacity. The ultimate uplift capacity can be enhanced to a greater extent by increasing the surface roughness or by changing the orientation of the fibre.

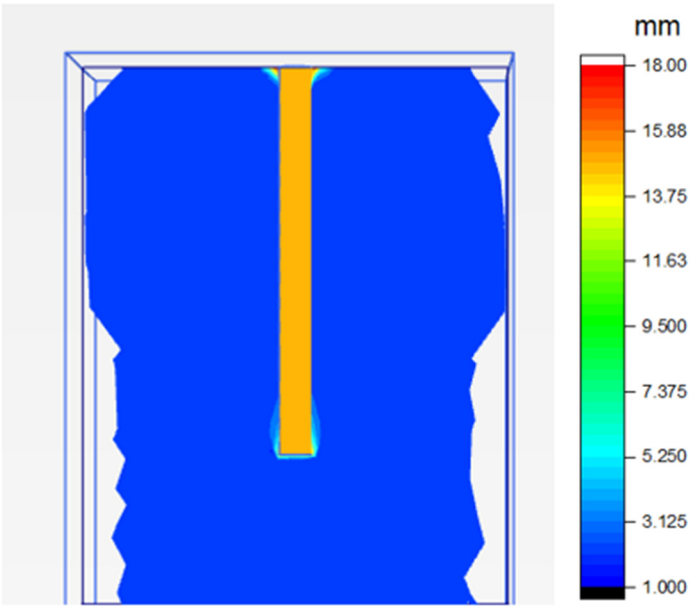

Figure 19. Displacement diagram of the pile during the uplift.

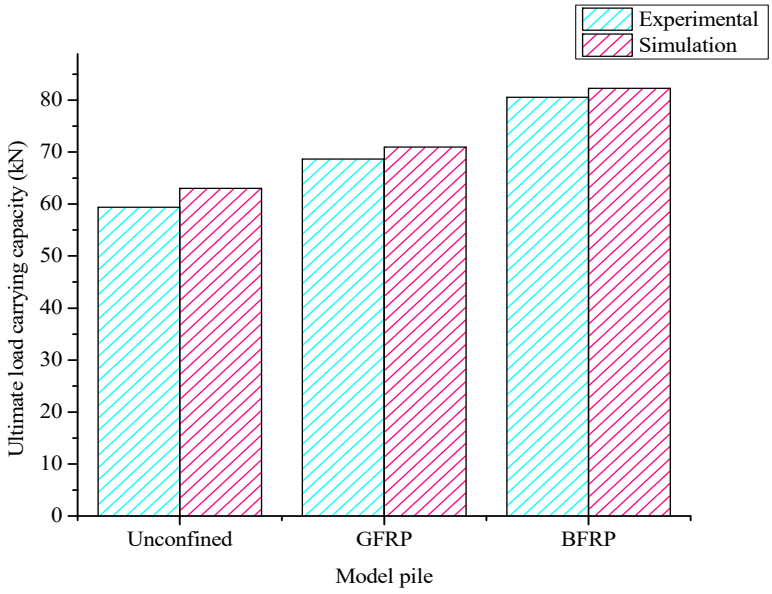

Figure 20. Uplift capacity of the piles.

An important part of the design of the FRP piles is the accurate modelling of the pile's structural resistance. In the numerical modelling, the authors observed that the confinement effect on the concrete and pile boundary conditions played a critical role in simulating the uplift capacity of the pile. Furthermore, the material properties, such as specific weight and primarily the elastic modulus of the composite material, had critical effect on improving the model's development process and its output. In the analysis, the pile was modelled with linear elastic properties and a nonlinear analysis of the FRP

composites for improving the accuracy of the finite element model. In the model study, the uplift capacity was found to follow a pattern similar to the experimental results for both the FRPs. The ultimate uplift capacity was observed as 82.3 kN and 71 kN for the GFRP and BFRP wrapping, respectively, from the model (Table 9). The experimental and finite element simulation results were observed to have a closer relation. All of the simulated results were found to have a degree of agreement not less than 87%. It was also found that the degree of agreement for the dry condition was very much closer to the experiments (not less than 94%).

Table 9. Uplift capacity – Experiment vs Model.

Type of Wraps	Load-Carrying Capacity (kN)					
	Dry Condition			Submerged Condition		
	Experimental (P_{exp})	Finite Element Analysis (P_{fea})	P_{exp}/P_{fea}	Experimental (P_{exp})	Finite Element Analysis (P_{fea})	P_{exp}/P_{fea}
Unconfined	59.4	63.0	0.94	37.80	42.77	0.88
GFRP	68.64	71.0	0.97	42.60	49.23	0.87
BFRP	80.52	82.3	0.98	49.38	52.84	0.93

In addition, the developed model allows for the use of any structural commercial program to determine the FRP load capacity. It can be concluded that the FRP load capacity problem can be effectively solved through structural responses and geotechnical characteristics without a complex model such as the disturbed state concept [48] by modifying the combined modulus of the elasticity of the pile using the finite element method.

4. Conclusions

An analytical method for calculating the characteristics of an FRP-confined pile foundation based on the interaction characteristics of the polymer was presented in this paper. A comparison of the results obtained by the proposed method with those provided by an uplift resistance test using experimental and finite element analysis was elaborated. The experimental results obtained were compared with the numerical results and found to be in good agreement. Based on the experimental and finite elemental study, the following conclusions are drawn:

- The glass fibre-reinforced polymer (GFRP) and basalt fibre-reinforced polymer (BFRP) showed a higher uplift capacity than the unconfined RC pile due to the increase in the angle of the interfacial friction;
- Based on the field experiments, the ultimate uplift capacity was observed as 80.52 kN and 68.64 kN for the piles with the GFRP and BFRP wraps, respectively, which is 35.56% and 15.56% higher than the unconfined pile;
- The increase in the uplift load-carrying capacity was predominantly influenced by the pile surface texture which was dictated by the weaving of the fabric, imparting higher skin frictional resistance on the interface. The BFRP fibre imparted a higher surface roughness compared to the GFRP and, hence, resulted in a higher uplift capacity;
- The ultimate uplift capacity can be enhanced to a greater extent by a fibre orientation perpendicular to the loading direction compared to a parallel orientation. However, for improving the uplift load resistance of the piles, providing protrusions or bulbs at different heights of the piles can be provided to increase the uplift resistance.

It is further recommended to undertake experiments to identify the behavioural improvements with the use of fibre wraps on piles subjected to different forms of loadings, such as lateral, cyclic, fatigue, and impact loads, to ensure the suitability of the fibre laminates for the strengthening of the piles. The effect of the protrusions in the form of bulbs and screw teeth at varying depths should be experimented to understand the shape effects.

Author Contributions: Conceptualization, M.Y.M.M. and M.M.; methodology, M.Y.M.M., M.M. and B.S.S.; software, M.Y.M.M.; validation, M.Y.M.M. and M.M.; formal analysis, M.Y.M.M.; investigation, M.Y.M.M.; resources, M.Y.M.M.; data curation, M.Y.M.M. and B.S.S.; writing—original draft preparation, M.Y.M.M.; writing—review and editing, M.Y.M.M., M.M. and B.S.S.; supervision, M.M. All authors have read and agreed to the published version of the manuscript.

Funding: This research received no external funding.

Institutional Review Board Statement: Not applicable.

Informed Consent Statement: Not applicable.

Data Availability Statement: The data related to the present study are available in the manuscript.

Conflicts of Interest: The authors declare no conflict of interest.

References

1. Micheal Tomlinson, J.W. *Pile Design and Construction Practice*, 5th ed.; Taylor & Francis: Oxfordshire, UK, 2008; ISBN 0203964292.
2. Chen, L.; Chong, J.; Pang, L.; Zhang, C. Lateral capacity of a two-pile group foundation model located near slope in sand. *Ocean Eng.* **2022**, *266*, 112847. [CrossRef]
3. Wang, F.; Shao, J.; Li, W.; Wang, Y.; Wang, L.; Liu, H. Study on the Effect of Pile Foundation Reinforcement of Embankment on Slope of Soft Soil. *Sustainability* **2022**, *14*, 14359. [CrossRef]
4. Liu, H.; Li, J.; Yang, X.; Chen, L.; Wu, W.; Wen, M.; Jiang, M.; Guo, C. Lateral Dynamic Response of Offshore Pipe Piles Considering Effect of Superstructure. *Energies* **2022**, *15*, 6759. [CrossRef]
5. Ingham, T.J. Analysis of the Million Dollar Bridge for seismic retrofit. *Comput. Struct.* **2003**, *81*, 673–679. [CrossRef]
6. Sakellariadis, L.; Marin, A.; Anastasopoulos, I. Widening of Existing Motorway Bridges: Pile Group Retrofit versus Nonlinear Pile–Soil Response. *J. Geotech. Geoenvironmental Eng.* **2019**, *145*, 04019107. [CrossRef]
7. Visuvasam, J.A.; Chandrasekaran, S.S. Effect of Spacing and Slenderness Ratio of Piles on the Seismic Behavior of Building Frames. *Buildings* **2022**, *12*, 2050. [CrossRef]
8. Alyavdin, D.; Belyakov, V.; Levin, A.; Alekseev, A.; Grechishcheva, E.; Kozlova, O.; Makhota, R. Reline Jacket: Efficient Reduction of Frost-Heave Uplift of Piles in Warming Permafrost. *Geosciences* **2022**, *12*, 313. [CrossRef]
9. Murugan, M.; Muthukkumaran, K.; Natarajan, C. FRP-Strengthened RC Piles. I: Piles under Static Lateral Loads. *J. Perform. Constr. Facil.* **2017**, *31*, 04017003. [CrossRef]
10. Sen, R.; Mullins, G. Application of FRP composites for underwater piles repair. *Compos. Part B Eng.* **2007**, *38*, 751–758. [CrossRef]
11. Chellapandian, M.; Prakash, S.S.; Sharma, A. Experimental and finite element studies on the flexural behavior of reinforced concrete elements strengthened with hybrid FRP technique. *Compos. Struct.* **2018**, *208*, 466–478. [CrossRef]
12. Chellapandian, M.; Jain, S.; Prakash, S.S.; Sharma, A. Effect of Cyclic Damage on the Performance of RC Square Columns Strengthened Using Hybrid FRP Composites under Axial Compression. *Fibers* **2019**, *7*, 90. [CrossRef]
13. Lu, Y.; Abuel-Naga, H.; Shaia, H.A.; Shang, Z. Preliminary Study on the Behaviour of Fibre-Reinforced Polymer Piles in Sandy Soils. *Buildings* **2022**, *12*, 1144. [CrossRef]
14. Faleschini, F.; Gonzalez-Libreros, J.; Zanini, M.A.; Hofer, L.; Sneed, L.; Pellegrino, C. Repair of severely-damaged RC exterior beam-column joints with FRP and FRCM composites. *Compos. Struct.* **2018**, *207*, 352–363. [CrossRef]
15. Mohammed, A.A.; Manalo, A.C.; Ferdous, W.; Zhuge, Y.; Vijay, P.V.; Alkinani, A.Q.; Fam, A. State-of-the-art of prefabricated FRP composite jackets for structural repair. *Eng. Sci. Technol. Int. J.* **2020**, *23*, 1244–1258. [CrossRef]
16. Vijay, P.V.; Soti, P.R.; GangaRao, H.V.S.; Lampo, R.G.; Clarkson, J.D. Repair and Strengthening of Submerged Steel Piles Using GFRP Composites. *J. Bridg. Eng.* **2016**, *21*, 04016038. [CrossRef]
17. Xian, G.; Guo, R.; Li, C.; Wang, Y. Mechanical performance evolution and life prediction of prestressed CFRP plate exposed to hygrothermal and freeze-thaw environments. *Compos. Struct.* **2022**, *293*, 115719. [CrossRef]
18. Zhou, P.; Li, C.; Bai, Y.; Dong, S.; Xian, G.; Vedernikov, A.; Akhatov, I.; Safonov, A.; Yue, Q. Durability study on the interlaminar shear behavior of glass-fibre reinforced polypropylene (GFRPP) bars for marine applications. *Constr. Build. Mater.* **2022**, *349*, 128694. [CrossRef]
19. Guo, R.; Li, C.; Xian, G. Water absorption and long-term thermal and mechanical properties of carbon/glass hybrid rod for bridge cable. *Eng. Struct.* **2023**, *274*, 115176. [CrossRef]
20. Sharma, S.S.; Dave, U.V.; Solanki, H. FRP Wrapping for RC Columns with Varying Corner Radii. *Procedia Eng.* **2013**, *51*, 220–229. [CrossRef]
21. Vijayan, D.S.; Mohan, A.; Daniel, J.J.; Gokulnath, V.; Saravanan, B.; Kumar, P.D. Experimental Investigation on the Ecofriendly External Wrapping of Glass Fiber Reinforced Polymer in Concrete Columns. *Adv. Mater. Sci. Eng.* **2021**, *2021*, 2909033. [CrossRef]
22. Khandelwal, S.; Rhee, K.Y. Recent advances in basalt-fiber-reinforced composites: Tailoring the fiber-matrix interface. *Compos. Part B Eng.* **2020**, *192*, 108011. [CrossRef]
23. Ramaswamy, A.; Chachithanantham, S.; Arumugam, S. Performance of BFRP Retrofitted RCC Piles Subjected to Axial Loads. *Adv. Mater. Sci. Eng.* **2014**, *2014*, 323909. [CrossRef]

24. Teshager, D.K.; Kabeta, W. Review on experimental and finite element analysis of vertically loaded piles. *Int. J. Adv. Res. Eng. Appl. Sci.* **2020**, *9*, 1–11.
25. González, F.; Carbonari, S.; Padrón, L.A.; Morici, M.; Aznárez, J.J.; Dezi, F.; Maeso, O.; Leoni, G. Benefits of inclined pile foundations in earthquake resistant design of bridges. *Eng. Struct.* **2019**, *203*, 109873. [CrossRef]
26. Meyerhof, G.G. The Uplift Capacity of Foundations Under Oblique Loads. *Can. Geotech. J.* **1973**, *10*, 64–70. [CrossRef]
27. Chattopadhyay, B.C.; Pise, P.J. Uplift Capacity of Driven Piles in Sand. *J. Inst. Eng. Civ. Eng. Div.* **1987**, *68*, 89–91.
28. Rowe, R.K.; Davis, E.H. The Behaviour of Anchor Plates in Sand. *Geotechnique* **1982**, *32*, 25–41. [CrossRef]
29. Murray, E.J.; Geddes, J.D. Uplift of Anchor Plates in Sand. *J. Geotech. Eng.* **1988**, *114*, 1461–1462. [CrossRef]
30. Ilamparuthi, K.; Dickin, E.A.; Muthukrisnaiah, K. Experimental investigation of the uplift behaviour of circular plate anchors embedded in sand. *Can. Geotech. J.* **2002**, *39*, 648–664. [CrossRef]
31. *IS 12269*; 2013 Ordinary Portland Cement, 53 Grade Specification. Bureau Indian Standards: New Delhi, India, 2013; pp. 1–14.
32. *IS 383:2016*; Coarse and Fine Aggregate for Concrete-Specification. Bureau of Indian Standards: New Delhi, India, 2016; pp. 1–18.
33. *IS:2386 (Part I)*; Method of Test for Aggregate for Concrete (Particle Size and Shape). Bureau Indian Standards: New Delhi, India, 1963.
34. *IS 10262*; Guidelines for Concrete Mix Design Proportioning. Bureau Indian Standards: New Delhi, India, 2009; pp. 1–14.
35. Maheswaran, J.; Chellapandian, M.; Arunachelam, N. Retrofitting of severely damaged reinforced concrete members using fiber reinforced polymers: A comprehensive review. *Structures* **2022**, *38*, 1257–1276. [CrossRef]
36. *IS 516*; Method of Tests for Strength of Concrete. Bureau Indian Standards: New Delhi, India, 1959; pp. 1–30.
37. *IS 5816*; Indian Standard Splitting Tensile Strength of Concrete- Method of Test. Bureau Indian Standards: New Delhi, India, 1999; pp. 1–14.
38. *IS 456*; Plain Concrete and Reinforced Concrete. Bureau Indian Standards: New Delhi, India, 2000; pp. 1–114.
39. Bowles, J.E. *Foundation Analysis and Design*, 5th ed.; The McGraw-Hill Companies, Inc.: New York, NY, USA, 1995; ISBN 0-07-912247-7.
40. *IS:2911 (Part1/Section 2)*; Design and Construction of Pile Foundations-Code of Practice. Bureau of Indian Standards: New Delhi, India, 2010; Volume 2911, p. 2911.
41. *IS:2911 (Part 4)*; Code of Practice for Design and Construction of Pile Foundations. Part 4: Load Test on Piles. Bureau of Indian Standards: New Delhi, India, 1985.
42. Ni, P.; Mangalathu, S.; Mei, G.; Zhao, Y. Permeable piles: An alternative to improve the performance of driven piles. *Comput. Geotech.* **2017**, *84*, 78–87. [CrossRef]
43. Brinkgreve, R.B.J.; Kumarswamy, S.; Swolfs, W.M.; Waterman, D.; Chesaru, A.; Bonnier, P.G.; Haxaire, A. *Plaxis 2015*; Plaxis BV: Delft, The Netherlands, 2016; ISBN 9789076016184.
44. Rohith, M.; Mouli, S.; Balunaini, U. Interference of Two Closely-Spaced Footings on Finite Sand Layer. *Geotech. Eng.* **2018**, *49*, 128–135.
45. Ghosh, P.; Mukherjee, S.; Roy, N.; Banerjee, S. Response of Single Pile to Lateral Load with Constant Uplift. In *Advances in Computer Methods and Geomechanics*; Springer: Berlin/Heidelberg, Germany, 2020; pp. 283–298.
46. Nasrollahzadeh, E.; Hataf, N. Experimental and numerical study on the bearing capacity of single and groups of tapered and cylindrical piles in sand. *Int. J. Geotech. Eng.* **2019**, *16*, 426–437. [CrossRef]
47. Das, B.M. Procedure for Estimation of Uplift Capacity of Rough Piles. *Soils Found.* **1983**, *23*, 122–126. [CrossRef]
48. Desai, C.S.; Pradhan, S.K.; Cohen, D. Cyclic Testing and Constitutive Modeling of Saturated Sand–Concrete Interfaces Using the Disturbed State Concept. *Int. J. Géoméch.* **2005**, *5*, 286–294. [CrossRef]